SCIENTIFIC REPORTS

OPEN

SUBJECT AREAS:
GROWTH AND DEVELOPMENT
STRUCTURAL BIOLOGY
SIGNAL TRANSDUCTION
BIOCHEMISTRY

Received
24 August 2011

Accepted
7 October 2011

Published
28 October 2011

Correspondence and requests for materials should be addressed to T.Y. (tyamazak@nias.affrc.go.jp)

* The first two authors contributed equally to this work.

Structural mechanism of JH delivery in hemolymph by JHBP of silkworm, *Bombyx mori*

Rintaro Suzuki[1]*, Zui Fujimoto[1]*, Takahiro Shiotsuki[2], Wataru Tsuchiya[1], Mitsuru Momma[1], Akira Tase[1], Mitsuhiro Miyazawa[3] & Toshimasa Yamazaki[1]

[1]Biomolecular Research Unit, National Institute of Agrobiological Sciences, 2-1-2 Kannondai, Tsukuba, Ibaraki 305-8602, Japan, [2]Insect Growth Regulation Research Unit, National Institute of Agrobiological Sciences, 1-2 Owashi, Tsukuba, Ibaraki 305-8634, Japan, [3]Insect Mimetics Research Unit, National Institute of Agrobiological Sciences, 1-2 Owashi, Tsukuba, Ibaraki 305-8634, Japan.

Juvenile hormone (JH) plays crucial roles in many aspects of the insect life. All the JH actions are initiated by transport of JH in the hemolymph as a complex with JH-binding protein (JHBP) to target tissues. Here, we report structural mechanism of JH delivery by JHBP based upon the crystal and solution structures of apo and JH-bound JHBP. In solution, apo-JHBP exists in equilibrium of multiple conformations with different orientations of the gate helix for the hormone-binding pocket ranging from closed to open forms. JH-binding to the gate-open form results in the fully closed JHBP-JH complex structure where the bound JH is completely buried inside the protein. JH-bound JHBP opens the gate helix to release the bound hormone likely by sensing the less polar environment at the membrane surface of target cells. This is the first report that provides structural insight into JH signaling.

Juvenile hormones (JHs) are acyclic sesquiterpenoids which contain an α,β-unsaturated methyl ester and a terpenoid backbone with an epoxide distal to the ester. Both the ester and epoxide groups are required for hormone regulatory functions. JH regulates many processes, including the growth, development, metamorphosis and reproduction of insects[1,2]. The diversity of JH-mediated physiological effects suggests that target cells may respond to the hormone directly by gene expression and/or via a second messenger[3,4]. In any cases, the first essential process for JH actions is transport of the JH molecule from *corpora allata* cells where the hormone is synthesized to the proper sites of its actions in target cells. In Lepidoptera which major agricultural pests belong to, a specific 30 kDa JH-binding protein (JHBP) is responsible for this JH delivery process[5]. Several lines of evidence indicate that almost every molecule of JH in hemolymph is bound to JHBP[6–8]. In this sense, JHBP is the most important protein that regulates the JH signaling. Complex formation provides protection of the chemically labile JH against nonspecific enzymatic degradation and/or sequestration, and is crucial for effective signaling by low amounts of the hormone.

JHBP has high affinity and enantioselectivity for naturally occurring JHs[5,9,10], and JHBPs from various lepidopteran species share 40% to 50% amino-acid sequence identity but show no homology with other proteins (Supplementary Fig. S1). The only exception is the family of insect Takeout proteins which share limited sequence similarity (< 20%) with JHBPs. The Takeout proteins have been established as being critically involved in important aspects of insect behavior, but their actual functions remain unclear[11–14]. Although the crystal structure of *Galleria mellonella* JHBP has recently been determined[15], no structural information about JHBP-ligand interactions is available to date. The lack of structural knowledge of the JHBP-JH complex prevents our understanding of the ligand specificity and the protection mechanism of JH by JHBP. Besides protection and transport of JH, ligand uptake and targeted release are the fundamental functional features of JHBP, but neither process is well understood as yet. Many of the most critical questions regarding the delivery of JH by JHBP will require structural elucidation of ligand-bound and ligand-free proteins.

Here we report the crystal structures of apo- and JH II-bound JHBP from the silkworm, *Bombyx mori*. We have also determined the solution structure of the JHBP-JH III complex by NMR spectroscopy. The first three-dimensional structures of the JHBP-JH complexes both in the crystalline and solution states, together with subsequent biochemical assays, allowed us to elucidate detailed molecular mechanism of JH recognition by JHBP that clearly explains the ligand specificity and JH protection mechanism of JHBP. Comparison of the

apo- and JH-bound structures suggests that the uptake and release of JH are regulated by opening and closing of α-helix on the JH-binding pocket that functions as a gate to sense ligand entry. In the apo form of JHBP in the crystalline state, the gate resides in an open conformation which permits access of JH to the preserved hormone-binding pocket. In solution, the gate of the apo-JHBP is highly mobile and undergoes chemical exchange between multiple conformational states, including the gate-open conformation seen in the crystalline state and the gate-closed conformations similar to those observed for the JH II- and JH III-bound forms. Such conformational dynamics of the gate of the apo-JHBP is silenced by JH-binding. Addition of more than 30% of ethanol to the JHBP-JH complex resulted in dissociation of the bound-JH molecule, suggesting that the JH-bound JHBP opens the gate helix to release the bound hormone likely by sensing reduction of the dielectric constant at the membrane surface of target cells. Based on the results in this report, we propose structural mechanism of JH delivery by JHBP in hemolymph, the first essential process of the JH signal transfer.

Results

Structures of apo- and JH II-bound JHBP in the crystalline states. We solved crystal structures of the apo- and JH II-bound *B. mori* JHBP both at 2.2 Å resolution (Fig. 1 and refinement statistics in Supplementary Table S1). The recombinant *B. mori* JHBP adopts the same elongated barrel fold, comprising a long helix α3 wrapped in a highly curved anti-parallel β-sheet, as the native *G. mellonella* JHBP[15]. Nearly the same folds are shared by an insect Takeout protein[14] as well as by mammalian lipid carrier proteins such as human bacterial/permeability-increasing protein (BPI)[16] and cholesteryl ester transfer protein (CETP)[17] (Supplementary Fig. S2). BPI and CETP have two homologous domains in tandem, each of which has a JHBP-like fold.

The central part of the β-sheet in JHBP is five-stranded, whereas only four strands are present at both ends. In the closed structure of the JH II-bound form (Fig. 1a), shorter helices α1 and α2 join the four-stranded parts of the β-sheet to form a wrap structure around the C- and N-terminal ends of the α3-helix, respectively, whereas in the open structure of the apo-form the α1 helix dissociates from the β-sheet (Fig. 1b). JHBP has two hydrophobic pockets at each end of the elongated structure. Among these two, only the pocket near the C-terminus of α3 accommodates one molecule of JH while the other pocket remains empty in the JHBP-JH complex (Fig. 1a). The JH-binding pocket is completely closed at the middle of the protein structure by hydrogen-bond networked side chains of Gln73 in the β2a-β2b loop, Thr91 in β3, and Tyr201 in α3, together with Leu70 and Val204. The three hydrogen-bonded residues are strictly conserved for JHBPs but are diversified for Takeout proteins (Supplementary Fig. S1), suggesting that existence of two separated pockets is a common feature for the lepidopteran JHBP family whereas the Takeout family has a long continuous tunnel for ligand binding (Supplementary Fig. S2).

Gate-latch mechanism for hormone uptake by JHBP. Comparison of the apo- and JH-bound JHBP structures suggests that a gate and latch mechanism is employed for hormone binding. The apo-JHBP structure is very similar to the JH II-bound structure with respect to the core of the protein (residues 32–210), demonstrating that the JH-binding pocket is preserved in the apo-protein (Fig. 1c). However, significant deviations are observed for the entry of the JH-binding pocket which is surrounded by a gate helix α1 along with the N-terminal arm on one side, and on the other side, a latch-like region formed by the C-terminal tail. The positions of residues in the C-terminal tail do not change substantially between the apo- and JH-bound structures. In contrast, the largest difference is the length and orientation of the gate α1 helix which is 1.5-turn shorter at its N-terminus in the apo-form than in the JH-bound form. In the apo-JHBP structure (Fig. 1c), the location of the α1 helix generates a wide open conformation, which permits access of JH to the hormone-binding site that is completely exposed to the solvent region. JH binding induces a dramatic change in the orientation of α1, which swings toward the pocket about 70° from the position of the corresponding helix in the apo-structure (Fig. 1c). The hinge point for the movement of α1 is marked by sharp differences in (ϕ, ψ) angles of Thr28, Ser29, Lys30, and Gly31 near the C-terminus of α1 (Supplementary Table S2). The α1-β1 connecting appendix-like hairpin loop, composed of highly conserved GIPQYDIWPIDP sequence (Supplementary Fig. S1), serves as a gatepost of α1 (Fig. 1c). This hairpin loop is maintained in a close proximity to α3 through a hydrogen-bond network formed by Asp36 and Trp38 in the loop and His206 and Asn207 in α3, as well as π-π stacking interactions between the aromatic side chains of Trp38 and His206 (Fig. 1d). It is noteworthy that the C-terminal end of this hairpin has a structurally conserved *cis* peptide bond between Asp41 and Pro42.

In the gate-closed structure of the JHBP-JH II complex, the α1 helix associates with β2 strand mainly by polar interactions, most of them mediated by water molecules (Fig. 1e). Only one direct interaction is formed between the side chains of Glu26 in α1 and Lys71 in the β2a-β2b loop. A network of water molecules is favorably coordinated between the side chains of Ser18 and Glu22 in α1 and the Asn72 side chain, as well as the backbones of Gln73 and Ile75. The closed conformation is further stabilized by hydrophobic and polar interactions between residues in α1 and the α,β-unsaturated ester moiety of JH as discussed below. These JH-contacting residues are exposed to the solvent in the apo-structure. The closure of the ligand entry gate α1 brings the N-terminal arm, invisible in the apo-structure, in a close proximity of the C-terminal tail, leading to formation of two hydrogen bonds between Cys9 NH and Phe220 CO and between Glu222 NH and Cys9 CO in the presence of JH (Fig. 1d). The structure of the C-terminal tail is further stabilized by hydrogen bonds between Ala217 NH and Gln140 CO and between His141 $N^{\delta 1}$ and Ala212 CO. The N-terminal arm is further linked to α1 via a disulfide bond between Cys9 and Cys16. This disulfide bond is reported to be essential for the JH-binding ability of JHBP[18]. The hydrogen-bonded N-terminal arm and C-terminal tail serve as a latch and seal the bound JH molecule preventing its exposure to the solvent (Fig. 1d and Fig. 2a). In this binding mode, the JHBP-bound hormone is completely buried inside the carrier protein and thus protected from unfavorable nonspecific absorption and enzymatic degradation during its transport in the hemolymph.

Molecular basis for hormone recognition by JHBP. The structure of the JHBP-JH II complex shows that JHBP recognizes the characteristic shape and functional groups of JH with high specificity by means of hydrogen-bond networks and hydrophobic contacts. The JH-binding pocket of JHBP matches almost accurately the van der Waals surface of the bound JH II molecule (Fig. 2a). To fit in the pocket, the JH II molecule assumes an L-shaped structure, which is accomplished by successive *gauch*(+) conformations about the C3-C4 and C4-C5 bonds (Fig. 2b–d). In such an L-shaped structure, the distance between the functionally important ester and epoxide is approximately 9 Å. Although the positions of the epoxide and the ester groups are nearly identical for the two structures of the bound JH II molecules in the two JHBP-JH II complexes present in the crystal asymmetric unit, torsion angles about the C7-C8 and C9-C10 bonds are different from each other due to a crankshaft-like motion (Fig. 2d).

In the JHBP-JH II complex, there is a slight open space around the methyl group (R2) attached to C7 while the ethyl group (R3) attached to C11 makes perfect contacts with the hydrophobic wall of the pocket (Fig. 2a). This observation explains the binding affinity of JH homologs for *B. mori* JHBP in the order of JH I > JH II > JH III[19]. There is a large open space around the methyl ester of the bound

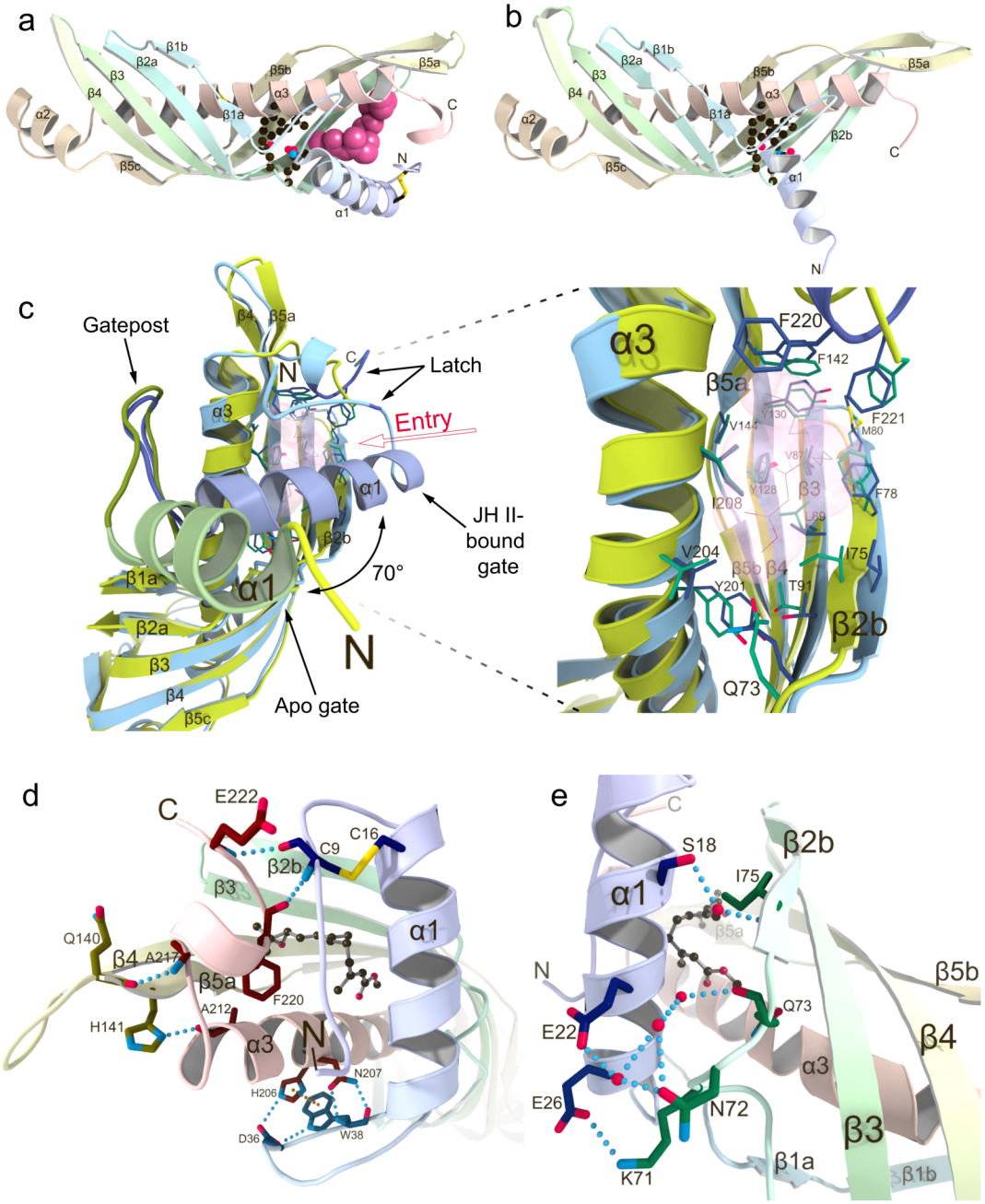

Figure 1 | Comparison of crystal structures of *Bombyx mori* JHBP in the apo- and JH-bound forms reveals a gate-latch mechanism for JH binding to JHBP. (a) The crystal structure of JHBP in complex with JH II. The bound JH II molecule is shown as a space-filling model. Side chains of residues forming the bottom wall of the JH-binding pocket are shown as ball-and-stick models and disulfide bonds as stick models. (b) The crystal structure of apo-JHBP. Side chains of residues forming the bottom wall of the JH-binding pocket are shown as ball-and-stick models and disulfide bonds as stick models. (c) Close-up views of the JH entry site in the overlay of the apo- (green) and JH II-bound (light blue) JHBP structures with the transparent surface of the JH II, showing movement of the gate α1 helix upon JH-binding as well as the conserved positioning of the JH-interacting residues in the protein core of the both forms. (d) Interactions between the latch-forming N-terminal arm and C-terminal tail that are further linked to the gate α1 helix and the protein core, respectively. Also shown is association of the α1-β1 connecting appendix-like loop with α3-helix. Key residues for interactions are shown as stick models with hydrogen bonds (light-blue dotted lines) and π-π stacking (orange dotted line). (e) Association of the gate α1 helix with β2 strand in the JHBP-JH II complex. The side chains of key residues for interactions are shown as stick models with hydrogen bonds (light-blue dotted lines). Water molecules are shown as red spheres and JH II as a ball-and-stick model.

JH. Filling of this open space by a slightly longer ester group (up to three carbons) could result in closer contacts of the ligand molecule with the bottom wall of the pocket. This scenario might explain the previous results that substitution of the methyl ester of JH with ethyl, propyl or allyl esters enhances binding affinity, whereas introduction of more bulky substituents such as propargyl, butyl or benzyl esters reduces binding affinity[20].

The epoxide of JH is confined in a hydrophobic cage and stabilized mainly by CH-π stacking interactions between methyl and ethyl groups attached to C11 with the aromatic side chains of Tyr130, Phe142 and Phe220 (Fig. 3a). Adding to these interactions, the hydroxyl group of Tyr128 forms a direct hydrogen bond with the expoxy oxygen of JH. This hydrogen bond explains the high enantioselectivity of JHBP for the *R*-configuration at C10 of JH[21]. The

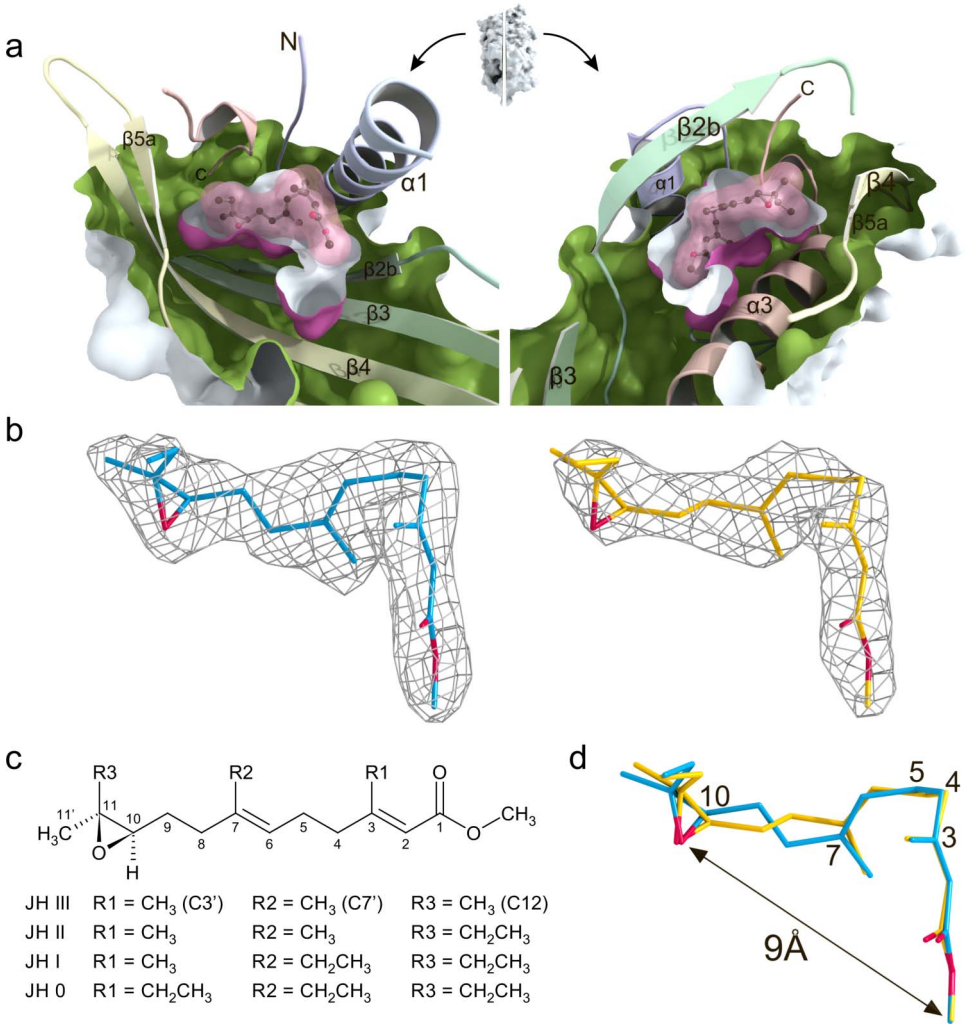

Figure 2 | Mechanism for JH protection by JHBP and conformations of the JHBP-bound JH. (a) View of the JH-binding pocket of the crystal structure of the JHBP-JH II complex. A surface representation of the JH II-bound JHBP was split vertically through the JH-binding pocket perpendicular to the page. The interior of the protein and the exterior of the pocket are colored green and purple, respectively. The halves produced from the split were rotated in opposite directions to create the view shown. The bound JH II molecule is shown as a ball-and-stick model with its molecular surface (pink). (b) The |Fo| – |Fc| omit electron density maps of two JH II molecules in the two JHBP-JH II complexes present in the crystal asymmetric unit. The amplitudes |Fc| and the phase angles were calculated from the partial structure in the absence of the JH II molecules. The contour levels are 3.0 σ (molecule A, blue) and 2.5 σ (molecule B, yellow). Oxygen atoms are shown in red. (c) Chemical structures of juvenile hormone homologs showing the numbering scheme used to identify the heavy atoms of the molecule. (d) Comparison of L-shaped structures of the JHBP-bound JH II molecules (molecules A in blue and B in yellow) in the two JHBP-JH II complexes present in the crystal asymmetric unit. Oxygen atoms are shown in red.

ester side of JH is stabilized by CH-π interaction between the C3' methyl group of JH and the aromatic ring of Phe24 in α1 and van der Waals interactions with side chains of Thr21 and Leu25 in α1, Leu89 in β3, Val204 and Ile208 in α3, and Leu6 in the N-terminal arm (Fig. 3b). In addition, the carbonyl oxygen of the ester is linked to Thr28 in α1, Val204 and Asn207 in α3 by means of two water molecules. Ile208, together with Leu17 in α1 and Phe78 in β2b, also make van der Waals contacts with the terpenoid backbone of JH. Most of the JH-interacting residues identified here are strictly conserved or conservatively substituted within the lepidopteran JHBP family except for Leu6 and Val204 (Supplementary Fig. S1).

To assess further the functional relevance of the hormone-protein contacts identified in our structural analyses, we constructed 23 JHBP single-mutants for 20 key interacting residues and examined their JH-binding activity *in vitro*. As shown in Fig. 3c, ten mutants harboring an alanine substitution show very little or no activity (<10%), confirming that Leu17, Phe24 and Leu25 in α1, Phe78 and Met80 in β2b, Tyr128 and Tyr130 in β4, Phe142 in β5, Ile208 in α3, and Phe220 in the C-terminal tail are essential for JH binding. Importance of the hydrogen bond from the Tyr128 O$^{\eta}$H to the epoxy oxygen of JH is confirmed by a loss of binding activity for the Y128F mutant. Furthermore, remarkably reduced affinity observed for the T91V and Q73A mutants demonstrate that the hydrogen-bond network formed by Gln73, Thr91 and Tyr201 at the bottom of the JH-binding pocket is also essential for the JH binding activity of JHBP.

JH-induced silencing of conformational dynamics in the hormone binding site of JHBP in solution. To gain insight into structures of the apo- and JH-bound JHBP in solution, we used NMR spectroscopy. JHBP in complex with JH III displayed an excellent ^{1}H-^{15}N heteronuclear single quantum coherence (HSQC) spectrum (Supplementary Fig. S3a), for which a single set of signals was observed for the entire protein sequence. On the basis of nearly complete signal assignments[22], we have successfully determined a high-precision NMR solution structure of the JHBP-JH III complex (Supplementary Table S3 and Fig. S4) which closely resembles the

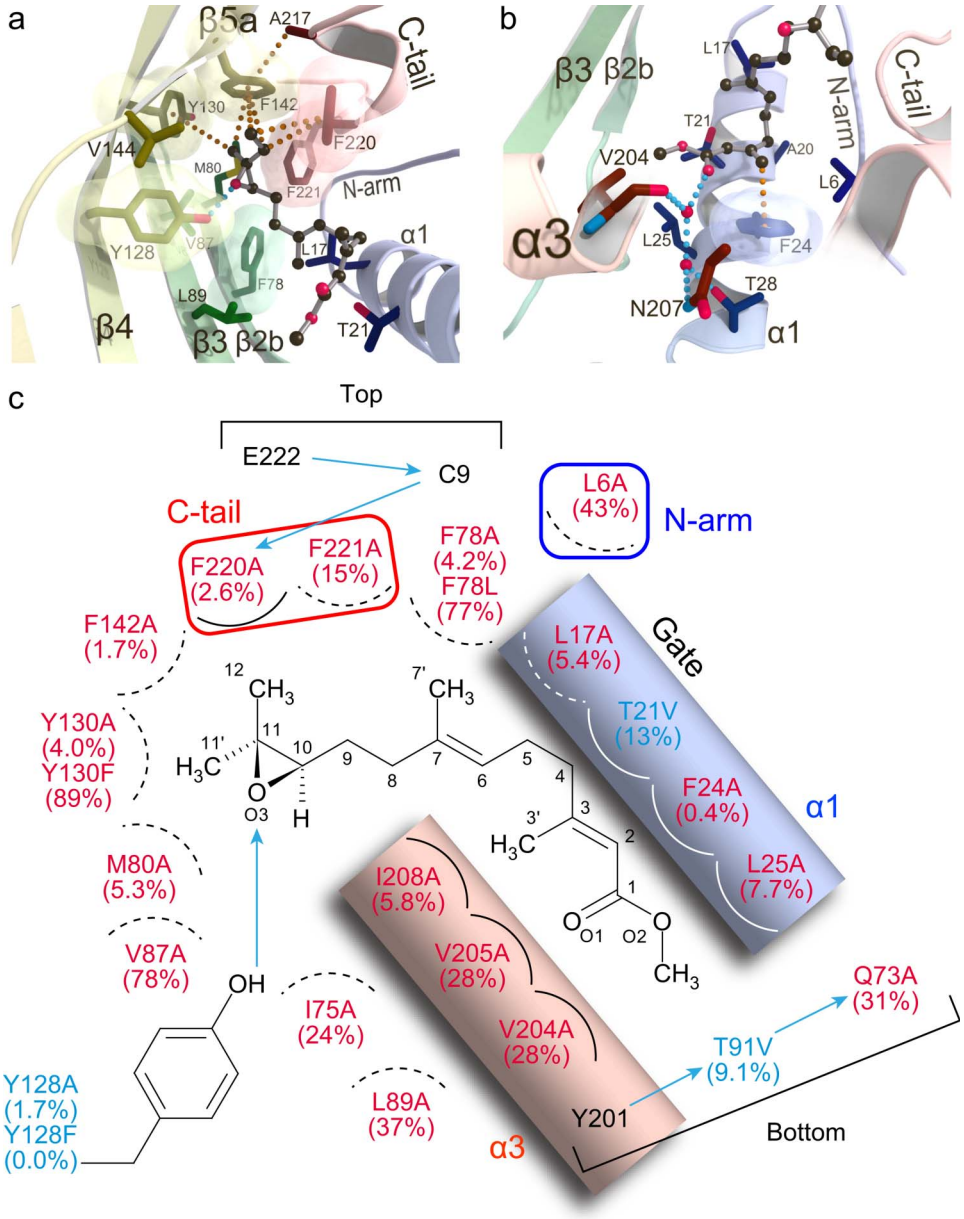

Figure 3 | **Molecular basis for JH recognition by JHBP.** Interactions of JHBP with the epoxy moiety (a) and the ester moiety (b) of JH II in the crystalline state. Residues involved in the recognition are shown as stick models and JH II as a ball-and-stick model. The transparent molecular surfaces of aromatic residues are also shown. Hydrogen bonds and stacking interactions are indicated by light blue and orange dotted lines, respectively. (c) Schematic diagram of the JH recognition mechanism by JHBP. JH III binding affinities of the single-mutant JHBPs relative to the wild-type protein are shown in the parentheses. Polar and non-polar interactions are indicated by arrows and circular arcs, respectively. The interactions occurring behind JH III are shown as dashed lines. Mutants with substitutions of residues involved in non-polar interactions alone and in both polar and non-polar interactions are shown in red and blue, respectively.

crystal structure of the JHBP-JH II complex (Fig. 4a), indicating excellent correspondence between the recognition features observed in the crystalline and solution states.

A ^{1}H-^{15}N HSQC spectrum of the ligand-free JHBP maintained a well-dispersed nature of signals, but only 60% of the theoretically expected signals were observed (Supplementray Fig. S3b). Almost all the observed signals arise from residues localized in a half of the elongated molecular structure, on the side opposite from the JH-binding pocket. Chemical shifts of these residues are essentially the same in the apo- and JH III-bound forms (Supplementary Fig. S3c), indicating that these residues assume nearly the same conformations in both forms (Fig. 4b). Disappearance of 40% of the signals suggests that residues of the apo-JHBP surrounding the JH binding site exhibit conformational dynamics due to multiple conformations in solution. In the crystalline states, the structure of the protein core is well conserved both in the gate-open apo-form and in the gate-closed JH II-bound form while the orientation of the α1 helix is significantly different in these two forms as mentioned above. In addition, a gate-closed conformation has been reported for *G. mellonella* JHBP with JH binding pocket empty[15]. Taking these data together, we conclude that the gate α1 conformations ranging from the fully closed to open forms are present in the apo-JHBP in solution, while the protein core is well maintained in all of these structures and that JH binding silences conformational dynamics of the α1 gate and leads to the formation of the unique closed conformation seen in the JHBP-JH complex.

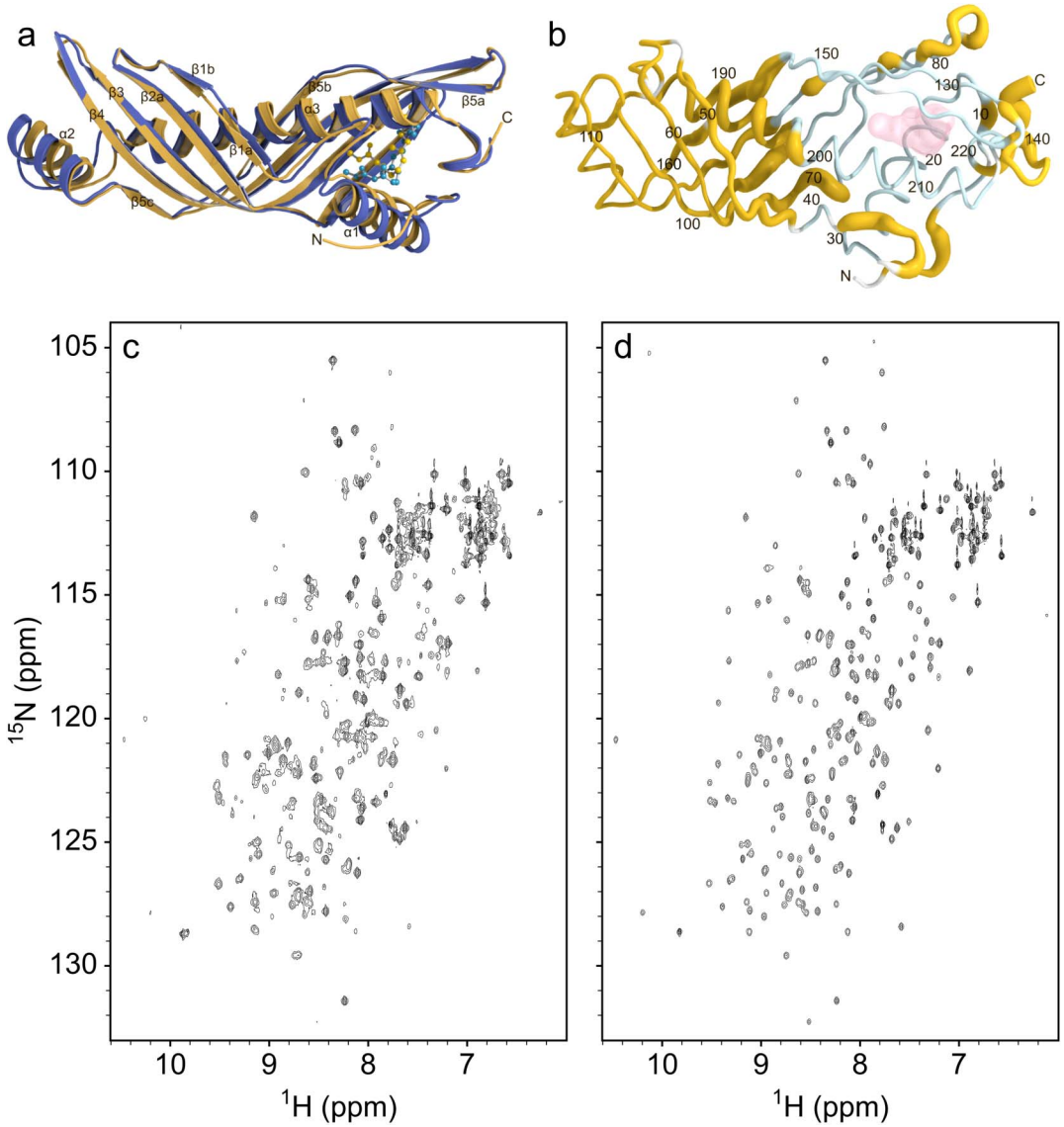

Figure 4 | JH-induced silencing of conformational dynamics of JHBP in solution and ethanol-induced release of the bound-JH from the complex. (a) The NMR solution structure of *B. mori* JHBP-JH III complex (yellow) is overlaid with the crystal structure of the JHBP-JH II complex (blue). The bound JH molecules are shown as ball-and-stick models. (b) Sausage model of the NMR solution structure of the JH III-bound JHBP where the diameter is proportional to the weighted chemical shift difference between the apo- and JH III-bound proteins in solution, calculated with the function $\Delta\delta = [\Delta\delta_{HN}{}^2 + (\Delta\delta_{15N}/5)^2]^{1/2}$. Shown in light-blue are residues for which NMR signals were not observed for the apoprotein due to chemical exchange between multiple conformational states on a time-scale of NMR chemical shifts. Proline and N-terminal residues are shown in white. The JH III molecule is shown as transparent surface. (c) ^{1}H-^{15}N HSQC spectrum of the JHBP-JH III complex (200 μM) in 50 mM sodium phosphate buffer, pH 6 after the treatment with 30% ethanol, collected at 35°C on a Bruker DMX 750 spectrometer. The sample was prepared as follows. The JHBP-JH III complex was diluted to 10 μM in 50 mM sodium phosphate buffer, pH 6, in the presence of 30% ethanol at 4°C for one hour. The JH III molecules released from the complex were removed by solvent exchange with the same solvent using Amicon Ultra-15 centrifuge concentrator with 5 kDa cutoff, to avoid the rebinding of the unbound JH III to the protein. The residual ethanol was removed by exhaustive solvent exchange into the buffer used for the NMR measurement. The resultant protein sample provided the HSQC spectrum which displays two sets of signals, one set from the ligand-free JHBP and the other from the JHBP-JH III complex. The same treatment of the JHBP-JH III complex with 10% ethanol did not cause the unbinding of JH III from the complex, as evidenced by no spectral changes from the original JHBP-JH III complex (d).

Dissociation of the bound JH from the JHBP complex. *G. mellonella* JHBP shows the highest binding of JH at pH 7 and no binding at pH 4[23]. We observed a similar pH-dependent JH binding profile for *B. mori* JHBP. A rather steep decrease in JH binding activity below the pH optimum is analogous to that observed for pheromone binding in insect pheromone-binding proteins (PBPs) which transport the hydrophobic pheromones through the aqueous environment to pheromone receptors. It has been proposed that PBPs deliver pheromones to the membrane-bound odorant receptors by a pH-dependent conformational change, with a major transition between pH 6 and 5, the acidic environment expected in the vicinity of the membranes housing the receptors[24]. To examine whether JHBP would release JH at lower pH, we measured a series of NMR spectra at pH 4 for the preformed JHBP-JH III complex prepared at pH 6. With the exception of several solvent-exposed Asp, Glu, and their surrounding residues, most of residues show small differences in backbone amide chemical shifts between pH 6 and pH 4 (Supplementary Fig. S5). More importantly, intermolecular NOEs between JH III and JHBP detected at pH 6 were also observed at pH 4. These results clearly demonstrate that JH once bound to JHBP

at physiological pH does not dissociate from the complex when the pH is lowered, leading to a conclusion that, unlike the PBP-pheromone complex, targeted release of JH from the JHBP complex *in vivo* seems to require the assistance of external factors other than pH.

Our result obtained during the apo-JHBP crystal formation may indicate a specific environmental factor that causes the ligand release from the JHBP complex. These crystals were obtained by crystallizing the preformed complex with methoprene acid (MetA), an acid derivative of methoprene which functions as a JH-related growth regulator for insects, using a high concentration of PEG200 (50%) as a precipitant. NMR analysis of the JHBP-MetA complex suggests that MetA binds to the same site as JH and that the complex is stable in solution more than one year, therefore we believe that the JHBP-bound MetA molecule dissociates from the complex in the presence of PEG200 during crystallization. This result suggests that in a more hydrophobic environment the gate-open conformation, with the hydrophobic JH-binding site exposed to solvent, is preferred. Water-alcohol mixtures have been often used to monitor conformational changes of proteins near membrane surfaces[25], since the addition of alcohols lowers the dielectric constant of aqueous solutions of proteins. Using NMR spectroscopy, we indeed confirmed that the JHBP-JH III complex releases the bound-JH molecule by addition of more than 30% of ethanol (Fig. 4c,d), suggesting that the decreased dielectric constant in close proximity of the target membranes is a likely trigger for JH release from the complex by opening the gate α1 helix.

Discussion

JH regulates many different physiological processes essential to the insect life cycle. Since JH actions for the individual processes occur in tissue- and stage-specific manners, it is generally assumed that multiple number of JH receptors exist at the membranes and in cytosols and nuclei. In any cases, the first essential process for JH actions is a transport of the lipophilic JH molecule from the site of its synthesis to the proper sites of its actions in target tissues as a complex with the hemolymph JHBP. It is, therefore, essential for understanding JH actions to elucidate molecular mechanisms of uptake, recognition and targeted release of JH by JHBP. For this purpose, we utilized X-ray crystallography, solution NMR spectroscopy and *in vitro* JH binding assays.

Our results mentioned above enable us to outline the molecular mechanism of JH delivery by JHBP in hemolymph from the *corpora allata* cells where JH is synthesized to the target tissues as follows. The uptake and release of JH are regulated by the opening and closing of α1-helix on the JH-binding pocket that functions as a gate sensing the ligand entry. The apo-JHBP in hemolymph exists in equilibrium of multiple conformational states with different orientations of α1 ranging from the closed to open forms while the protein core structure is well maintained (Fig. 5a). In the less polar environment that may mimic the decreased dielectric constant near the membrane surface, the equilibrium shifts although not completely toward the gate-open conformations which permit access of JH to the highly hydrophobic hormone-binding site that is exposed to the solvent. At the *corpora allata* cell membrane, the epoxide of JH binds to the preformed hormone binding pocket of the apo-JHBP in the gate-open form first and then the gate helix α1 starts to close (Fig. 5b). During the closure of the gate, interactions of the α1 helix with the α,β-unsaturated ester moiety of JH are optimized. The closure of the ligand entry gate leads to formation of hydrogen bonds between the N-terminal arm and the C-terminal tail, resulting in the fully gate-closed JHBP-JH complex where the bound JH is completely buried inside the protein and thus protected from unfavorable nonspecific absorption and enzymatic degradation (Fig. 5c). When the JHBP-JH complex reaches to the target tissues, JHBP opens the

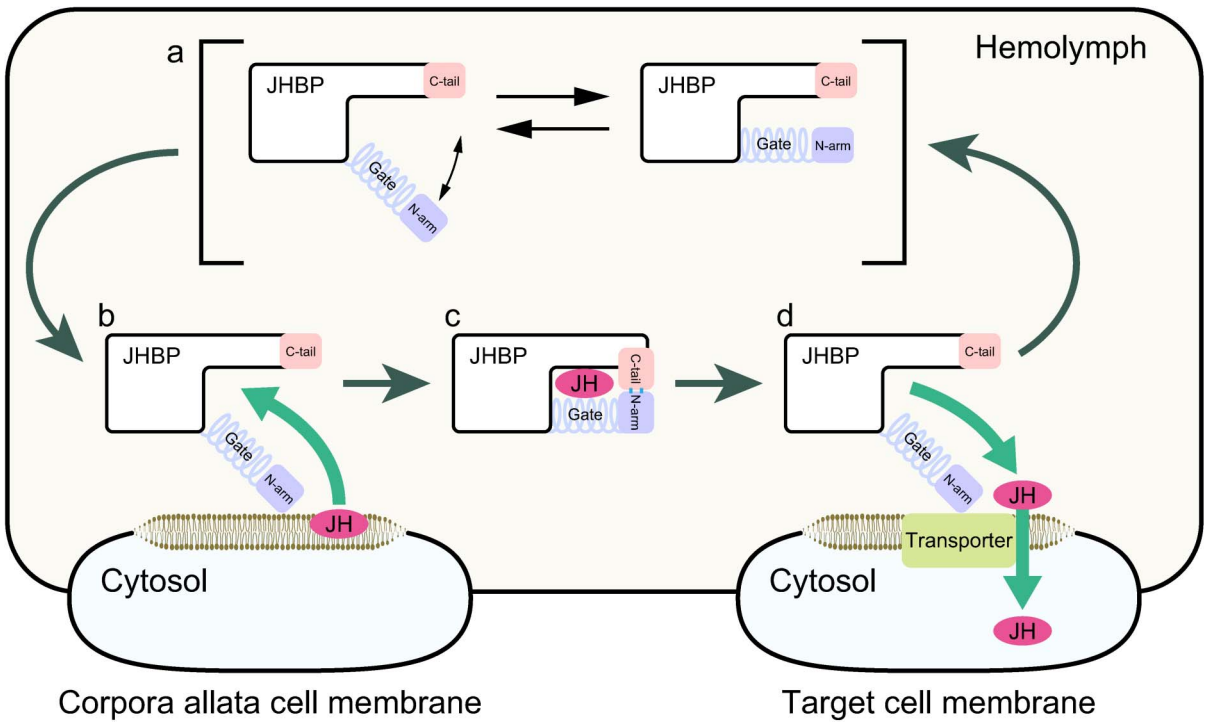

Figure 5 | Proposed mechanism for JHBP-mediated JH transport in the hemolymph from *corpora allata* cells to target cells. (a) In the ligand-free form, the JH carrier protein JHBP assumes various conformations of the gate α1 helix ranging from close to open forms. The open form presents a wide open, accessible cavity for JH with the flexible gate α1 and latch-like C-tail that guard the cavity's entrance. (b) JH binding at the membrance surface of the *corpora allata* cells where the JH is synthesized initiates an allosteric open-to-close transition, allowing the C-tail to form hydrogen bonds with the N-arm. (c) In the resulting fully closed JHBP-JH complex, the bound JH is completely buried inside the protein and protected from unfavorable nonspecific absorption and enzymatic degradation during the delivery to target cells in the hemolymph. (d) When the complex reaches to target cells, JHBP undergoes a conformational change from the fully closed to open forms that may be triggered by reduction of dielectric constant, and releases the bound JH.

α1-gate to release the bound-JH molecule (Fig. 5d). Our structural model outlining the molecular mechanism of JH delivery by JHBP in the hemolymph deepens our understanding of the JH signaling essential for the insect life cycle.

Finally, our structural investigation of the JHBP-JH complexes has practical importance for pest management. Because the hemolymph JHBP regulates the first process of the JH signaling and is highly specific to insects, JHBP is expected to be an excellent target for safe insect growth regulators (IGR). The detailed molecular mechanism of JH recognition by JHBP presented herein provides the first opportunity to rationalize computer-assisted design of IGRs which inhibit complex formation between JH and JHBP, and thus disrupt the JH signaling. Furthermore, the JHBP-JH interactions we identified should become fundamental data for JH recognition by other JH-specific proteins and could significantly assist in identification of undefined JH receptors.

Methods

Protein expression and purification. Mature JHBP from *Bombyx mori*, comprising residues 19–243 of the preprotein, was expressed as a GST-fusion protein in *E. coli* and purified as described previously[22,26]. Uniformly ^{15}N- and ^{13}C/^{15}N-labelled JHBP used for NMR studies was expressed in *E. coli* grown in C.H.L. medium enriched with ^{15}N and ^{13}C/^{15}N (Chlorella Industry) while SeMet-substituted protein used for the crystallographic study was expressed in *E. coli* strain B834 (DE3). Expression vectors for point mutants of JHBP were constructed by site-directed mutagenesis using PCR with the expression vector of the wild-type protein and the KODplus polymerase (TOYOBO). The desired mutant proteins were obtained by employing the same procedure used for the wild-type JHBP. Samples of JHBP complexed with either JH III (SIGMA), JH II (SciTech), or methoprene acid (MetA) (SIGMA) were obtained according to the procedure described previously[22].

Crystallization, data collection and structure determination. JHBP native and SeMet derivative crystals were obtained by the hanging-drop vapor-diffusion method at 20°C from solution containing 3 μL of apoprotein at 20 mg mL^{-1} in 2 mM Tris buffer, pH 8.0, and 1.5 μL of crystallant: 25% (±)-*2*-methyl-*2,4*-pentandiol (Hampton Research), 0.05 M zinc acetate (Wako) and 0.1 M sodium cacodylate buffer, pH 7.0 (Hampton Research). After a week, thin plate crystal clusters appeared and a typical crystal grew to the size of dimensions 500 × 20 × 10 μm. Crystals of JHBP-JH II complex were obtained by the sitting-drop vapor-diffusion method at 20°C from solution containing 1.5 μL of the complex at 18 mg mL^{-1} in 2 mM Tris buffer, pH 8.0, and 1.0 μL of crystallant: 15% PEG3350 (Hampton Research), 0.05 M zinc acetate and 0.1 M citrate buffer, pH 4.2 (Wako). After three months, tiny rod crystals appeared and a typical crystal grew to the size of dimensions 200 × 15 × 10 μm. Crystals of apo-JHBP were obtained by the sitting-drop vapor-diffusion method at 20°C from solution containing 0.3 μL of JHBP-MetA complex at 12.5 mg mL^{-1} in 2 mM Tris buffer, pH 8.0, and 0.3 μL of crystallant: 50% PEG200 (Hampton Research) and 0.1 M Tris buffer, pH 7.0 (Hampton Research). After two months, rod crystals appeared and a typical crystal grew to the size of dimensions 150 × 100 × 100 μm.

Diffraction data were collected at beamlines of the Photon Factory (PF), High Energy Accelerator Research Organization, Tsukuba, Japan. A single crystal was scooped in a nylon loop and directly flash-frozen in a nitrogen stream at 95 K. Native data were collected by CCD detectors (ADSC, CA, USA). Data were integrated and scaled using the program DENZO and *Scalepack* in the HKL2000 program suite[27]. Se-Met crystals belonged to the space group $P2_12_12_1$ and four molecules existed in the asymmetric unit with the Vm value of 3.0 Å^3 Da^{-1} and solvent content of 59.6%[28]. JHBP-JH II crystals belonged to the space group *C*2 and two molecules existed in the asymmetric unit with the Vm value of 2.9 Å^3 Da^{-1} and solvent content of 58.2%. Apo-JHBP crystals belonged to the space group $P6_322$ and one molecule existed in the asymmetric unit with the Vm value of 3.6 Å^3 Da^{-1} and solvent content of 65.7%. Anomalous dispersion data set for the SeMet crystal were collected at the selenium absorption edge of wavelength of 0.97888 Å.

Structural analysis of JHBP was conducted by SAD method using the SeMet data. Heavy atom search and initial phase calculation was conducted using the program SOLVE/RESOLVE[29,30]. A total of 16 heavy atom positions were determined, four of which were identified as the bound zinc ions. Initial model produced by RESOLVE indicated that the crystal contains four JHBP molecules in the asymmetric unit. Manual model rebuilding, introduction of water molecules, and molecular refinement were conducted using Coot[31] and Refmac5[32]. Successively, the JHBP-JH II complex structure was solved by the molecular replacement method using the resultant JHBP structure as a reference model by the program MOLREP[33]. The apo-JHBP structure was solved by the molecular replacement method using the JHBP-JHII complex structure as a reference model. The stereochemistry of the models was analyzed with the program RAMPAGE [34]. Data collection and structure refinement statistics are summarized in Supplementary Table S1.

NMR measurements and structure determination. Solutions used to record NMR spectra contained the free JHBP (0.6–1.0 mM) or the JHBP-JH III complex (0.6–1.0 mM) dissolved in 45 mM sodium phosphate buffer, pH 6.0, with 10% (v/v) D_2O. All NMR spectra were acquired at 35°C on a Bruker DMX 750 spectrometer equipped with a pulse-field gradient. The NMR spectra were processed by using NMRPipe software[35] and analyzed by using SPARKY 3 software (Goddard, T.D. and Kneller, D.G., University of California, San Francisco). The two-dimensional (2D) and three-dimensional (3D) experiments used to obtain signal assignments and interproton distance restraints for the protein have been described[22]. Slowly exchanging amide protons were identified by recording the 2D ^{1}H-^{15}N HSQC spectrum after the H_2O buffer was changed to a D_2O buffer. The proton signals of the JHBP-bound JH III were assigned using a combination of 2D ^{13}C-filtered (in F1 and F2) COSY and NOESY spectra[36], the latter obtained with a mixing time of 200 ms. The 3D ^{13}C-filtered/^{13}C-selected NOESY-HSQC spectrum with a mixing time of 200 ms was recorded to assign NOEs between JH III and the protein[37].

Structures of the JHBP-JH III complex were calculated by using the program CYANA, version 2.1[38]. Initial structures were calculated by using only uniquely assigned distance constraints. Subsequently, an iterative strategy was used for the structure refinement. In each round of structure refinement, the newly computed NMR structures were employed to assign additional NOE cross-peaks and to correct erroneous assignments. A JH III template, created by Discover 3 (Accelrys), was introduced to the CYANA residue library. By using the standard procedure for CYANA calculations with multiple molecules, the ligand was attached to the protein via one PL, two LL2 and 11 LL5 pseudoatom linkers of the CYANA library, spanning a maximal distance of ~128 Å from the C-terminus of the polypeptide chain to the CM atom of JH III. The JH III molecule was kept in the Z-configuration at the double bonds in positions 2 and 6, whereas rotatable single bonds and all methyl protons were allowed to rotate. In the final calculations using more than 12,000 distance and dihedral angle constraints, a total of 100 starting structures were generated randomly and the best 20 structures with the lowest energies were selected for the analysis. Excluding the first two residues originating from the expression vector, the structures are well aligned with backbone and nonhydrogen atom rmsd values of 0.32 ± 0.04 Å and 0.64 ± 0.05 Å, respectively. RAMPAGE[34] revealed 90.3%, 7.8%, and 1.8% of JHBP residues in the favored, allowed, and outlier regions of the (ϕ, ψ) map, respectively. Statistics for the NMR structure determination are summarized in Supplementary Table S3.

JH binding assay. The JH binding assay was conducted by using the described method[26]. For the assay, 20 mM Tris-HCl buffer, pH 7.9 supplemented with 5 mM magnesium acetate, 1 mM EDTA, 1 mM DTT, 1 mM PMSF, 2 μg/mL Leupeptines, 1 μg/mL Pepstatin A, 0.1 mM 3-octylthio-1,1,1-trifluoropropanone, and 0.1 mM diisopropyl fluorophosphates was used. Protein samples were incubated for 30 min at 4°C in a volume of 100 μL containing different amounts of unlabeled and ^{3}H-labeled JH III (62.90 GBq mmol^{-1}; New England Nuclear Chemicals). Unbound JH was removed by the addition of dextran-coated charcoal (DCC) solution (100 μL) and centrifugation for 2 min at 10,000*g*. The radioactivity of a 50 μL aliquot of the supernatant was measured using Perkin-Elmer Liquid Scintillation Counter (Tri-Carb 2900TR) for JH binding activity.

CD measurements. Circular dichroism (CD) spectra were recorded on a JASCO J-720W spectropolarimeter in the far-UV range (185–260 nm) using a 0.2 mm thermostatted cell at 25°C. Each protein was dissolved in 20 mM sodium phosphate buffer, pH 6.0, at protein concentration of 20 μM. Judging from far-UV CD spectra of JHBP single-mutants examined, none of the substitutions were associated with any significant changes in the protein structures at least at the secondary structure level.

1. Gilbert, L. I., Granger, N. A. & Roe, R. M. The juvenile hormones: historical facts and speculations on future research directions. *Insect Biochem. Mol. Biol.* **30**, 617–644 (2000).
2. Truman, I. W. & Riddiford, L. M. The origins of insect metamorphosis. *Nature* **401**, 447–452 (1999).
3. Sevala, V. L. & Davey, K. G. Juvenile hormone dependent phosphorylation of 100 kDa polypeptide is mediated by protein kinase C in the follicle cells of Phodnius prolixus. *Inver. Reprod. Dev.* **23**, 189–193 (1993).
4. Wyatt, G. R. & Davey, K. G. Cellular and molecular actions of juvenile hormone. Roles of juvenile hormone in adult insects. *Adv. Insect Physiol.* **26**, 155–261 (1996).
5. Kramer, K. J., Sanburg, L. L., Kézdy, F. J. & Law, J. H. The juvenile hormone binding protein in the hemolymph of *Manduca sexta* Johannson (*Lepidoptera: Sphingidae*). *Proc. Natl. Acad. Sci. USA* **71**, 493–497 (1974).
6. Trowell, S. C. High affinity juvenile hormone carrier protein in the haemolymph of insects. *Comp. Biochem. Physiol.* **103B**, 795–807 (1992).
7. Hidayat, P. & Goodman, W. G. Juvenile hormone and hemolymph juvenile hormone binding protein titers and their interaction in the hemolymph of hourth stadium *Manduca sexta*. *Insect Biochem. Mol. Biol.* **24**, 709–715 (1994).
8. Touhara, K., Lerro, K. A., Bonning, B. C. & Prestwich, G. D. Ligand binding by a recombinant insect juvenile hormone binding protein. *Biochemistry* **32**, 2068–2075 (1993).
9. Goodman, W., Schooley, D. A. & Gilbert, L. I. Specificity of the juvenile hormone binding protein: The geometrical isomers of juvenile hormone I. *Proc. Natl. Acad. Sci. USA* **75**, 185–189 (1978).

10. Prestwich, G. D. & Wawrzeńczyk, C. High specific activity enantiomerically enriched juvenile hormones: Synthesis and binding assay. *Proc. Natl. Acad. Sci. USA* **82**, 5290–5294 (1985).
11. Sarov-Blat, L., So, W. V., Liu, L. & Rosbash, M. The Drosophilla takeout gene is a novel molecule link between circadian rhythms and feeding behavior. *Cell* **101**, 647–656 (2000).
12. Du, J., Hiruma, K. & Riddiford, L. M. A novel gene in the takeout gene family is regulated by hormones and nutrients in Manduca larval epidermis. *Insect Biochem. Mol. Biol.* **33**, 803–814 (2003).
13. Saito, K. *et al.* Cloning and expression analysis of *takeout/JHBP* family genes of silkworm, *Bombyx mori*. *Insect Mol. Biol.* **15**, 245–251 (2006).
14. Hamiaux, C. *et al.* Crystal structure of *Epiphyas postvittana* Takeout 1 with bound ubiquinone supports a role as ligand carrier for Takeout proteins in insects. *J. Biol. Chem.* **284**, 3496–3503 (2009).
15. Kolodziejczyk, R. *et al.* Insect juvenile hormone binding protein shows ancestral fold present in human lipid-binding proteins. *J. Mol. Biol.* **377**, 870–881 (2008).
16. Beamer, L. J., Carroll, S. F. & Eisenberg, D. Crystal structure of human BPI and two bound phospholipids at 2.4 angstrome resolution. *Science* **276**, 1861–1864 (1977).
17. Qin, X. *et al.* Crystal structure of cholesteryl ester transfer protein reveals a long tunnel and four bound lipid molecules. *Nat. Struct. Mol. Biol.* **14**, 106–113 (2007).
18. Wojtasek, H. & Prestwich, G. D. Key disulfide bonds in an insect hormone binding protein: cDNA cloning of a juvenile hormone binding protein of *Heliothis virescens* and ligand binding by native and mutant forms. *Biochemistry* **34**, 5234–5241 (1995).
19. Kurata, K. *et al.* Purification and characterization of a juvenile hormone binding protein from hemolymph of the silkworm, *Bombyx mori*. *Comp. Biochem. Physiol.* **109B**, 105–114 (1994).
20. Goodman, W. G. & Chang, E. S. Chapter 14. Juvenile hormone cellular and hemolymph binding proteins. in *Comprehensive Insect Physiology, Biochemistry and Pharmacology. Vol. 7* (eds Kerkut, G. A. & Gilbert, L. I.) 491–510 (Pergamon Press, Oxford 1985).
21. Schooley, D. A., Bergot, J., Goodman, W. & Gilbert, L. I. Symthesis of both optical isomers of juvenile hormone III and their affinity for the JH-specific binding protein of *Manduca sexta*. *Biochem. Biophys. Res. Commun.* **81**, 743–749 (1978).
22. Suzuki, R., Tase, A., Fujimoto, Z., Shiotsuki, T. & Yamazaki, T. NMR assignments of juvenile hormone binding protein in complex with JH III. *Biomol. NMR Assign.* **3**, 73–76 (2009).
23. Ożyhar, A. & Kochman, M. Juvenile-hormone-binding protein from the hemolymph of *Galleria mellonella* (L). Isolation and characterization. *Eur. J. Biochem.* **162**, 675–682 (1987).
24. Horst, R. *et al.* NMR structure reveals intramolecular regulation mechanism for pheromone binding and release. *Proc. Natl. Acad. Sci. USA* **98**, 14374–14379 (2001).
25. Clément-Collin, V., Leroy, A., Monteilhet, C. & Aggerbeck, L. P. Mimicking lipid-binding-induced conformational changes in the human apolipoprotein E N-terminal receptor binding domain effects of low pH and propanol. *Eur. J. Biochem.* **264**, 358–368 (1999).
26. Vermunt, A. M. W. *et al.* The juvenile hormone binding protein of silkworm haemolymph: gene and functional analysis. *Insect Mol. Biol.* **10**, 147–154 (2001).
27. Otwinowski, Z. & Minor, W. Processing of X-ray diffraction data collected in oscillation mode. *Methods Enzymol.* **276**, 307–326 (1997).
28. Matthews, B. W. Solvent content of protein crystals. *J. Mol. Biol.* **33**, 491–497 (1968).
29. Terwilliger, T. C. Automated main-chain model building by template matching and iterative fragment extension. *Acta Crystallogr. D Biol. Crystallogr.* **59**, 38–44 (2003).
30. Terwilliger, T. C. & Berendzen, J. Automated MAD and MIR structure solution. *Acta Crystallogr. D Biol. Crystallogr.* **55**, 849–861 (1999).
31. Emsley, P. & Cowtan, K. Coot: model-building tools for molecular graphics. *Acta Crystallogr. B Biol. Crystallogr.* **60**, 2126–2132 (2004).
32. Murshews, G. N., Vagin, A. A. & Dodson, E. J. Refinement of macromolecular structures by the maximum-likelihood method. *Acta Crystallogr. B Biol. Crystallogr.* **53**, 240–255 (1997).
33. Vagin, A. & Teplyakov, A. *MOLREP*: an automated program for molecular replacement. *J. Appl. Crystallogr.* **30**, 1022–1025 (1997).
34. Lovell, S. C. *et al.* Structure validation by Cα geometry: ϕ, ψ and Cβ deviation. *Proteins* **50**, 437–450 (2003).
35. Delaglio, F. *et al.* NMRPipe: A multidimensional spectral processing system based on UNIX pipes. *J. Biomol. NMR* **6**, 277–293 (1995).
36. Ikura, M. & Bax, A. Isotope-filtered 2D NMR of a protein-peptide complex: Study of a skeletal muscle myosin light chain kinase fragment bound to calmodulin. *J. Am. Chem. Soc.* **114**, 2433–2440 (1992).
37. Burgering, M. J. *et al.* Observation of inter-subunit nuclear Overhauser effects in a dimeric protein. Application to the Arc repressor. *FEBS Lett.* **330**, 105–109 (1993).
38. Güntert, P., Mumenthaler, C. & Wüthrich, K. Torsion angle dynamics for NMR structure calculation with the new program DYANA. *J. Mol. Biol.* **273**, 283–298 (1997).

Acknowledgments

We thank the beamline researchers at Photon Factory and Spring-8 for the use of synchrotron radiation, H. Shindo and H. Wojtasek for discussions and critical comments on the manuscript. This work was supported in part by the Program for Promotion of Basic Research Activities for Innovative Bioscience (PROBRAIN) of Japan (to T.S.).

Author contributions

T.S. and T.Y. designed research, R.S., Z.F., T.S., W.T., M.M., A.T., M.M., and T.Y. performed the experiments, R.S., Z.F., T.S., and T.Y. analyzed data and T.Y. wrote the paper.

Additional information

Supplementary information accompanies this paper at http://www.nature.com/scientificreports

Atomic coordinates for the crystal structures of the JH II-bound and apo-JHBP and the solution structure of the JHBP-JH III complex have been deposited in the Protein Data Bank under the accession codes 3AOS, 3AOT, and 2RQF, respectively. The chemical shifts of the JHBP-JH III complex have been deposited in the BioMagResBank under the accession number 16021.

Competing financial interests: The authors declare no competing financial interests.

How to cite this article: Suzuki, R. *et al.* Structural mechanism of JH delivery in hemolymph by JHBP of silkworm, *Bombyx mori*. *Sci. Rep.* **1**, 133; DOI:10.1038/srep00133 (2011).